DOI: 10.1002/ejic.201101315

Structure–Photoluminescence Quenching Relationships of Iridium(III)–Tris(phenylpyridine) Complexes

Albert Ruggi,[a] Matteo Mauro,[b] Federico Polo,[b] David N. Reinhoudt,[a]
Luisa De Cola,*[a,b] and Aldrik H. Velders*[a,c]

Keywords: Iridium / Luminescence / Photoluminescence / Electrochemistry / Oxygen sensitivity / Density functional calculations

The synthesis, structural, photophysical, theoretical, and electrochemical characterization of four tris(2-phenylpyridine)-based Ir^{III} complexes are reported. The complexes were functionalized on the pyridine or on the phenyl rings with amide moieties substituted with a tris(ethyl)amine or ethyl groups, thereby yielding a family of compounds with hemicaged or open (without a capping unit but with similar functional groups on the ligand) structure. Within the context of the parent tris(2-phenylpyridine) and the full-cage iridium(III) complexes, structure–photoluminescence quenching relationships (SPQR) of the four complexes have been investigated. Luminescence quenching by oxygen has been studied with Stern–Volmer plots and through evaluation of the thermodynamic parameters involved in the quenching process. Density functional theory (DFT) and time-dependent DFT (TD-DFT) calculations have been performed on the complexes to gain insights into structural and electronic features and the nature of the excited states involved in the electronic absorption processes. Interestingly, shielding by the capping unit of moieties in which the LUMO orbital is mostly localized (on the pyridines) results in a dramatic 40 % decrease in oxygen quenching. Conversely, shielding of moieties in which the HOMO orbital is partially localized (on the phenyl rings) does not induce any change in the oxygen quenching degree. In both sets of compounds, the thermodynamic feasibility of oxygen quenching is the same for the hemicaged and open compounds, thus giving evidence of the structural origin of such quenching decrease. The SPQR opens up new routes to the design of tailored, more or less sensitive to oxygen, luminescent iridium complexes (e.g., for use as biolabels).

Introduction

Here we report the evidence for a structure-related shielding effect of the oxygen quenching of the luminescence of iridium(III)–tris(phenylpyridine) derivatives with hemicaged (i.e., with a capping unit) or open (i.e., without a capping unit) ligand structures. Iridium(III)-based luminophores have been the object of extensive studies in the last decades, especially due to their wide spectrum of possible applications.[1] The possibility of tuning the emission wavelength and the generally good emission properties make iridium(III) complexes ideal luminophores for the realization of organic light-emitting diodes (OLEDs),[2–4] and, more recently, also for several biomedical applications.[5–8] Moreover, the interaction of the excited states of transition-metal complexes with dioxygen (which results in the quenching of luminescence and the generation of highly reactive species like singlet oxygen and superoxide radical anion) has received increasing interest due to the possible realization of diagnostic and therapeutic agents.[9–14] Despite the studies directed towards understanding the theoretical relationship between structure and optical properties,[15,16] little is known about the structure–photoluminescence quenching relationship (SPQR) of these complexes. Transition-metal complexes with a cagelike ligand structure show a remarkable decrease in oxygen quenching. For instance, an Ru^{II} caged complex shows an 80% decrease in oxygen quenching with respect to $[Ru(bpy)_3]^{2+}$ (bpy = 2,2′-bipyridine),[17] and an Ir^{III} caged complex (**ii**, Scheme 1) that shows a similar decrease in oxygen quenching compared to the archetypical $[Ir(ppy)_3]$ (ppy = 2-phenylpyridine) (**i**, Scheme 1); this has been recently described by our group.[18] However, the origin of this quenching decrease is not yet clear. Moreover, many parameters (e.g., triplet energy, oxidation potential) are different from the caged to the respective reference complexes {i.e., $[Ru(bpy)_3]^{2+}$ and $[Ir(ppy)_3]$}, thus an univocal interpretation of the observed quenching decrease is not trivial.[13]

---

[a] Laboratory of Supramolecular Chemistry and Technology, MESA+ Institute for Nanotechnology, University of Twente, P. O. Box 217, Enschede, The Netherlands
E-mail: decola@uni-muenster.de
a.h.velders@utwente.nl
[b] Westfälische Wilhelms-Universität Münster, Physikalisches Institut and Center for Nanotechnology (CeNTech), Heisenbergstrasse 11, 48149 Münster, Germany
[c] BioMedical Chemistry, MIRA Institute of Biomedical Technology and Technical Medicine, University of Twente P. O. Box 217, Enschede, The Netherlands

Supporting information for this article is available on the WWW under http://dx.doi.org/10.1002/ejic.201101315.

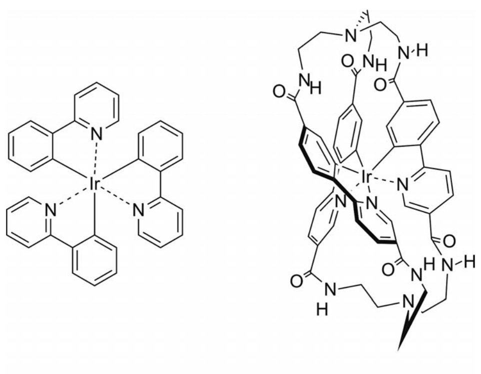

i ii

Scheme 1. Structure of the archetypical [Ir(ppy)$_3$] (**i**) and Ir caged complex (**ii**).

The remarkably low oxygen quenching of the luminescence observed for caged Ru^{II}[17] and Ir^{III}[18] complexes suggests a possible structural contribution to the shielding mechanism of the excited state (i.e., of the atoms on which the LUMO is mostly localized). A selective modification of the HOMO or of the LUMO properties in homoleptic [Ru(bpy)$_3$]$^{2+}$-like complexes is challenging, since the HOMO is mostly localized on the metal center and the LUMO is localized on the (symmetric) bipyridine ligands. On the other hand, for iridium complexes, and in particular for the [Ir(ppy)$_3$] derivatives, the 2-phenylpyridines are not symmetric and therefore are ideal candidates for a systematic study of the SPQR. In homoleptic [Ir(ppy)$_3$]-like complexes, the HOMO is usually localized on the metal ion and on the phenyl rings, whereas the LUMO (which can be considered a first approximation of the electronic distribution of the molecule in the excited state) is mostly localized on the pyridine rings.[1,15] The synthesis of caged complexes remains a great challenge and the versatility in tuning the ligands (and therefore properties) for these systems is complicated. Hemicaged systems are, on the other hand, much more accessible, and they might show similar shielding behavior but with a more accessible synthesis. In fact, upon introduction of suitable groups, either on the pyridine or phenyl side of the [Ir(ppy)] core, it is possible to selectively modify the electronic and/or shielding properties of the LUMO or HOMO, respectively, with a consequent change of the redox and optical properties like the emission energies.[1,16] In this paper we describe a series of Ir^{III}–tris(phenylpyridine) derivatives with a hemicaged or open structure in which we have selectively modified the HOMO and the LUMO orbitals.[11,19] Such a strategy allows us to understand the SPQR and to rationalize the behavior towards dioxygen quenching upon the shielding of the HOMO or of the LUMO.

More precisely, we present here the synthesis, characterization, and photophysical properties of a series of phenylpyridine-based Ir^{III} complexes functionalized with a tris(2-amidoethyl)amine capping unit or with an ethylamide moiety (i.e., with a hemicaged and open structure) (Scheme 2). The complexes possess a hemicaged (**1**, **3**) or an open (**2**, **4**) structure in which the substituents are on the pyridine (**1**, **2**) or on the phenyl (**3**, **4**) rings, respectively. These complexes are synthetically more accessible than the related fully caged system (**ii**),[18] and they show interesting structural shielding behavior. The introduction of a capping unit on the pyridine side (**1**) of the [Ir(ppy)$_3$] core, on which the LUMO orbital is mostly localized, induces a different shielding towards oxygen quenching than the open (unshielded) complex **2**. We in fact find that for **1** the quenching from dioxygen is lower than for complex **2**. On the contrary, the presence of a capping unit on the phenyl side (**3**), on which the HOMO is mostly localized, does not influence the degree of oxygen quenching and, therefore, the behavior of the hemicaged (**3**) and open (**4**) complexes towards oxygen quenching is the same. It is interesting to note that the molecules of each pair are in principle electronically and energetically equivalent in terms of excited state, and therefore the differences in their oxygen quenching can derive only from a structural effect. The oxygen quenching efficiency has been evaluated by Stern–Volmer analysis and compared with the thermodynamic parameters involved in the possible quenching pathways (i.e., energy transfer and electron transfer) to obtain clear evidence of the structure-related shielding against oxygen quenching. From this systematic study it was found that the introduction of a capping unit on the pyridine side of Ir^{III}–tris(phenylpyridine) derivatives induces a remarkable decrease in oxygen quenching with respect to the open (uncapped) structure, whereas only a minor decrease in oxygen quenching is observed upon introduction of the same capping unit on the phenyl side of Ir^{III}–tris(phenylpyridine) derivatives with respect to the corresponding open structure.

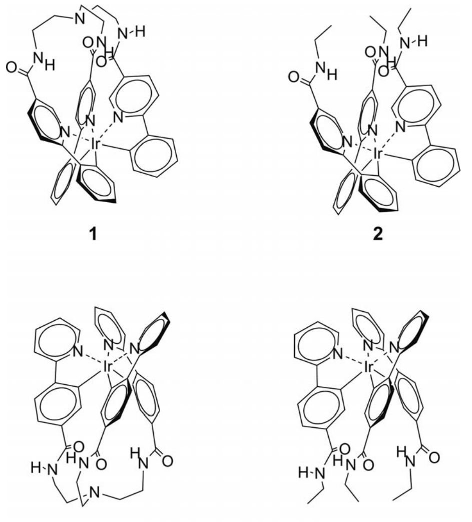

1 2

3 4

Scheme 2. Structures of the hemicaged (**1**, **3**) and open (**2**, **4**) Ir^{III} complexes.

Results and Discussion

Iridium(III) complexes **1**–**4** were synthesized according to the synthetic pathway shown in Scheme 3. The phenylpyridine-based building blocks were obtained upon Suzuki coupling[20] of bromonicotinic acid with phenylboronic acid (to give the phenylpyridine derivative **5**) or upon Suzuki coupling of 4-carboxymethylboronic acid with 2-bromopyridine (to give the phenylpyridine derivative **8**) with subsequent amide formation through amide coupling with, respectively, tris(2-aminoethyl)amine (Tren) (**6**, **9**) or ethylamine (**7**, **10**). The so-obtained ligands were treated with Ir^{III} to obtain the desired target complexes. The hemicaged complexes were synthesized by direct reaction of the suitable tripodal ligand (**6**, **9**) with $IrCl_3$ in the presence of CF_3CO_2Ag in ethylene glycol heated at reflux to give the hemicaged complexes **1** and **3**.[18] This strategy was not successful in the case of the open complexes; they were synthesized in two steps.[21] First the dichlorido-bridged dimer was obtained by reaction of the desired ligand (**7**, **10**) with $IrCl_3$ in 2-ethoxyethanol, and the so-obtained intermediate was treated with an excess amount of ligand in the presence of CF_3SO_3Ag in toluene heated at reflux (see Scheme 3) to give the open complexes **2** and **4**.

All the intermediates and the target complexes were characterized by IR and NMR (^1H and ^{13}C) spectroscopy and mass spectrometry, and the characteristic data are reported in the Experimental Section and in the Supporting Information. Complexes **1**–**4** show only one set of NMR spectroscopic signals for the three phenylpyridine ligands, which proves that the threefold symmetry expected for *fac* complexes is maintained. The ^1H NMR spectra of the hemicaged complexes **1** and **3** (see the Supporting Information) show, in addition, that upon formation of the iridium(III) complexes, the hemicage ligands become quite rigid: due to the hampered rotation around the C–C bond of the ethyl linkers, the four protons on each linker unit become magnetically nonequivalent, thereby resulting in four different multiplet signals in the ^1H NMR spectrum. A similar behavior has been observed for the hemicaged and caged Ir^{III} complexes previously described by our group.[18] Conversely, the ^1H NMR spectra of the open complexes **2** and **4** do not show any nonequivalent CH_2 or CH_3 protons, as expected for ethyl moieties with rotational freedom. The

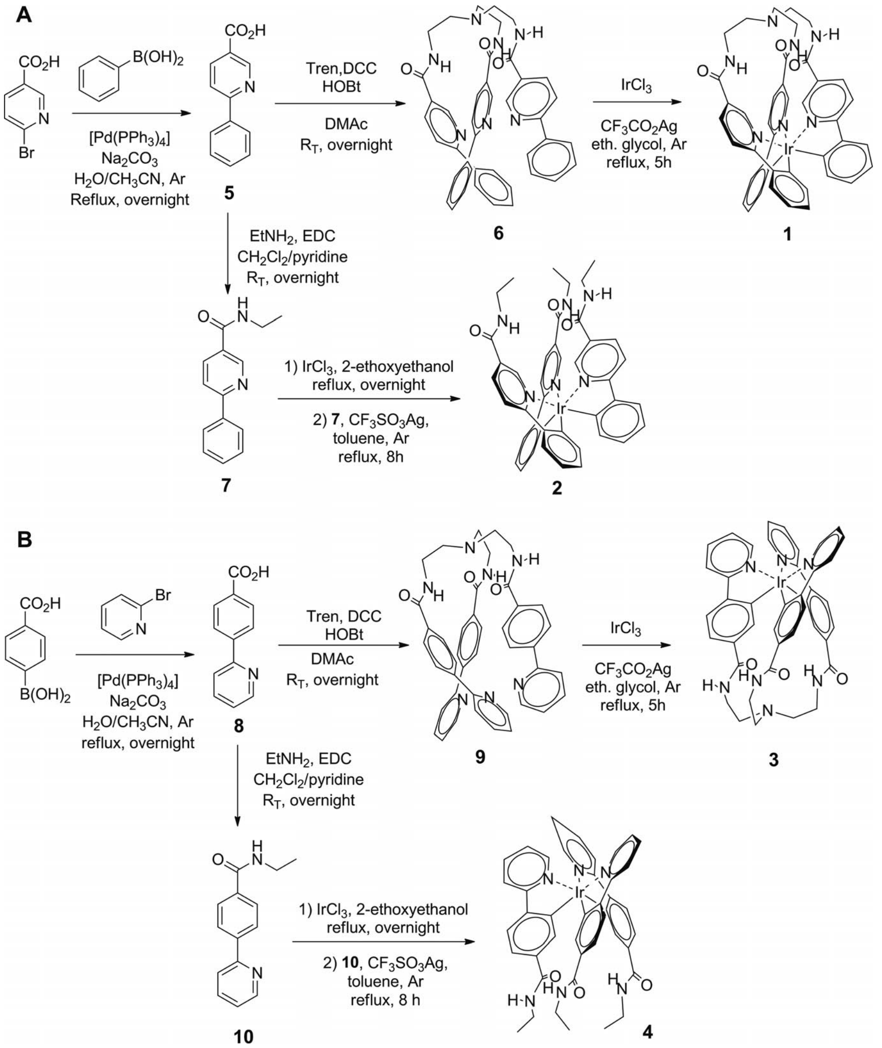

Scheme 3. Synthetic pathways for the synthesis of the hemicaged (**1**, **3**) and open (**2**, **4**) Ir^{III} complexes. The phenylpyridine derivatives **5** and **8** (obtained by Suzuki coupling) are coupled with Tren or ethylamine, thus giving the tripodal (**6**, **9**) or simple ligands (**7**, **10**), which are consecutively bound to Ir^{III}, thus giving the target molecules **1**–**4**.

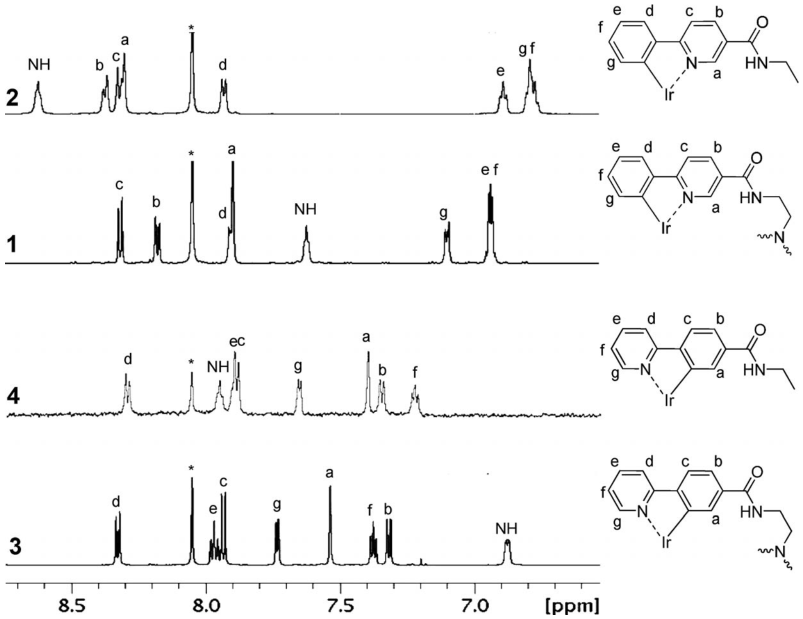

Figure 1. Aromatic region of the ^{1}H NMR spectra and peak assignment of hemicaged (**1**, **3**) and open (**2**, **4**) iridium(III) complexes; [D$_7$]DMF (* = residual solvent).

introduction of the capping unit induces a remarkable change in the signal of the amide proton (NH). Compared to the open complex **2**, the NH proton of the hemicaged complex **1** shows an upfield shift of 1 ppm (Figure 1). A similar upfield shift is also shown for the amide proton when comparing **4** to **3**. The observed change in the chemical shift of the amide proton (NH) is probably due to the change of the local polarity induced by the presence of the capping unit (vide infra). Interestingly, the proton Ha shows an upfield shift of 0.40 ppm from **2** to **1**, whereas only a modest (δ = 0.13 ppm) downfield shift is observed for Ha from **4** to **3**. The upfield shift of the Ha proton observed from **2** to **1** is possibly attributable to a magnetic shielding exerted by the aromatic rings located on the other branches of the molecule as a result of a higher degree of twisting of the helical structure of the [Ir(ppy)$_3$] core in the hemicage **1**: because of this higher twisting, the proton Ha in the hemicaged complex **1** faces the pyridine ring, thereby resulting in a downfield shift. On the other hand, the modest downfield shift observed for the proton Ha between **3** and **4** indicates that the structure of the [Ir(ppy)$_3$] core in the hemicaged complex **3** is only slightly distorted with respect to the open complex **4**.

To further investigate the geometry of the hemicaged complexes (**1**, **3**), a series of 2D NMR spectroscopic experiments (H,H-COSY, H,H-ROESY, H,C-HMBC and H,C-HMQC) was performed. The aromatic–aliphatic region of the ROESY spectrum of the hemicaged complex **1** (Figure 3) shows the coupling between the amide proton (NH) and three nonequivalent aliphatic protons on the ethyl linker (Hh, Hh′, Hi), analogously to what was found for the hemicaged complex previously described by our group.[18] The fourth proton (Hi′) is too far from the amide proton and does not give any through-space coupling. A similar coupling of the amide proton with three aliphatic protons on the ethyl linker was also observed for the hemicaged complex **3** (Figure 2), thus giving proof of the hemicaged structure of the two complexes **1** and **3**. In the aromatic region of the ROESY spectrum of the hemicaged complexes (Figure 2), the cross-peak between the protons Hc and Hd, which are located on the pyridine and phenyl ring, respectively, allows for a straightforward assignment of the remaining peaks from COSY data and the heteronuclear HMBC and HMQC experiments.

Careful analysis of the aromatic region of the ROESY spectrum of the hemicaged complex **1** (Figure 2) reveals the remarkable orientation of the amide moiety: the cross-peaks between the amide proton (NH) with both the internal (Ha) and the external (Hb) protons, *ortho* to the amide group, indicate that the NH group is not coplanar with the pyridine ring. To investigate the possibility of a certain degree of fluxionality in the capping unit of the hemicage system **1** to cause the characteristic two cross-peaks of the amide protons, variable-temperature (VT) NMR spectroscopy was performed. Neither the 1D VT measurements nor the ROESY performed at 250 K (see the Supporting Information) indicate the presence of more conformers of hemicage **1** to be present in solution on the NMR spectroscopic timescale.

A different behavior was observed for hemicage **3** (Figure 2), the amide proton of which gives a coupling only with the internal proton (Ha) on the phenyl ring; therefore, the NH group in **3** is likely coplanar with the phenyl ring and oriented towards the inner side of the molecule.

Two possible structures can be drawn for the hemicage **1** on the basis of the observed NOE cross-peaks. Either the entire amide moiety is not coplanar with the pyridine ring, or only the NH moiety of the amide group is bent out of

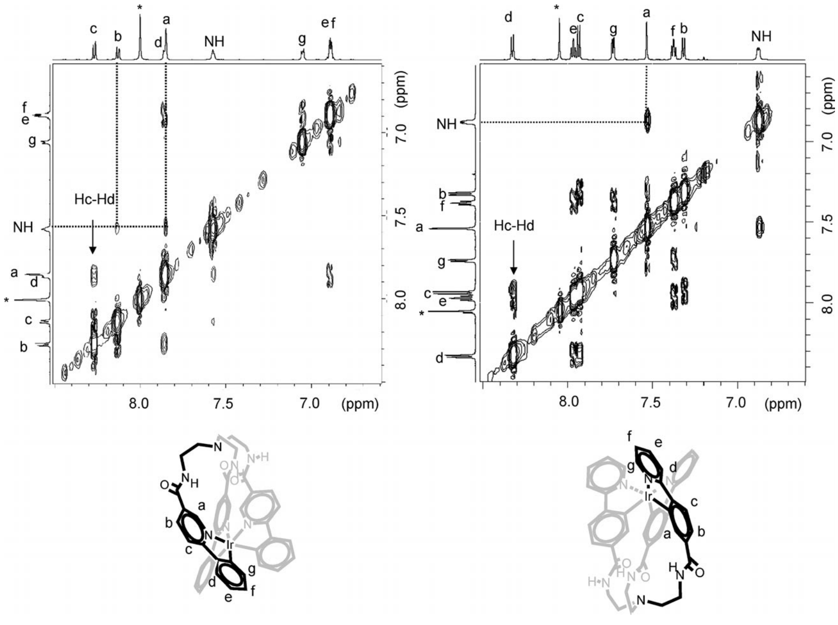

Figure 2. Downfield region of the H,H-ROESY spectra of the hemicaged complexes **1** (left) and **3** (right), recorded in [D$_7$]DMF. The residual solvent peaks are indicated with an asterisk.

the pyridine plane, with the carbonyl still coplanar with the pyridine. The first structure, with a lower conjugation of the pyridine ring and the carbonyl moiety, should influence the LUMO level less than the second structure in which the planarization of the system allows a stronger perturbation, and in particular a stabilization of the LUMO. Therefore, in the case of a lower conjugation of the pyridine ring and the carbonyl moiety, the emission of the hemicaged complex **1** is expected to be blueshifted compared to the open complex **2** (analogously to what has been observed in the case of the Ru^{II} caged complex).[17] Since complex **1** shows a small but clear bathochromic shift with respect to complex **2** (vide infra), it can be concluded that the carbonyl moiety of the amide group is conjugated with the pyridine ring. Therefore, most likely, the NH group is bent out of the pyridine plane.

Molecular structures of **1**–**4** were optimized at their electronic ground state (S$_0$) by means of DFT at the B3LYP/(6-31G(d,p) + SDD) level. The most meaningful computed geometrical parameters are reported in the Supporting Information (Table S7). The calculated S$_0$ structures are in good agreement when compared with experimental values of the closely related archetypical complex *fac*-[Ir(ppy)$_3$][22] within the known limitation of the density functional calculations used.[23] All the computed geometries investigated here possess a distorted octahedral arrangement around the heavy metal center, with C_3 point-group symmetry, and excellently reproduce the Ir–C bond length, with 2.036 Å being the value for **1** and 2.032–2.060 Å the theoretical and experimental values, respectively, whereas the Ir–N bond lengths are 2.192 (computed) and 2.071–2.095 Å (experimental).[24] It is also worth noting that the presence of the capping unit in the hemicaged complexes (**1** and **3**), seems not to affect the metal–ligand bond lengths with respect to the corresponding open derivatives (**2** and **4**), the computed bond displacements being ≤0.005 Å. As already reported by Nozaki et al.[23] and by Hay et al.,[15] Becke's three-parameter together with the Lee–Yang–Parr exchange correlation hybrid functional (namely, B3LYP) tends to slightly overestimate the Ir–N bond lengths. Also, a similar agreement between theoretical and experimental geometrical values can be envisaged for the complexes **2**–**4**. This finding nicely highlights the suitability of the employed theoretical model for describing the geometrical parameters of the complexes investigated here. Also, the B3LYP functional has been already widely proven to properly describe the electronic and optical properties of phosphorescent cyclometalated iridium complexes.[25,26] In Figure 3, the schematic representation of the energy levels of the orbitals

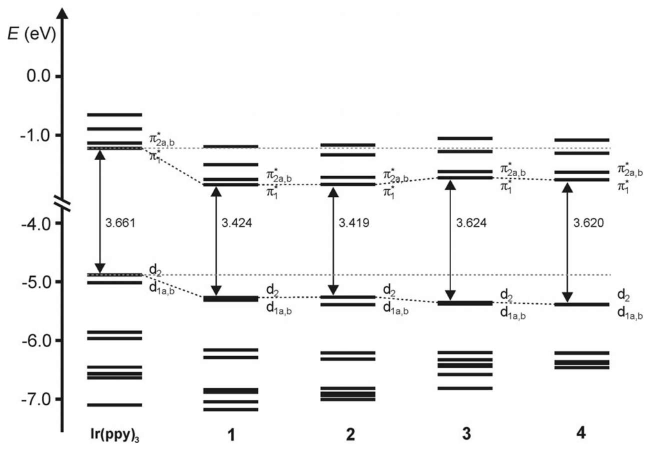

Figure 3. Partial molecular orbital diagram for complexes **1**–**4** and *fac*-[Ir(ppy)$_3$]. The arrows are intended to highlight the HOMO–LUMO energy gaps. All the DFT energy values are given in eV.

closer to the frontier region for the complexes **1**–**4** is reported, together with *fac*-[Ir(ppy)$_3$], which is used as reference. To provide deeper insight into the electronic structure of the complexes **1**–**4**, the isodensity surface plots of the most relevant Kohn–Sham molecular orbitals are shown in Figure 4 (for a more extended view, see Figures S5 and S6 in the Supporting Information). A list of the energies HOMO – 4 to LUMO + 4, along with the corresponding HOMO–LUMO energy gap, is reported in Table 1 (an extended version is available as Table S8 in the Supporting Information).

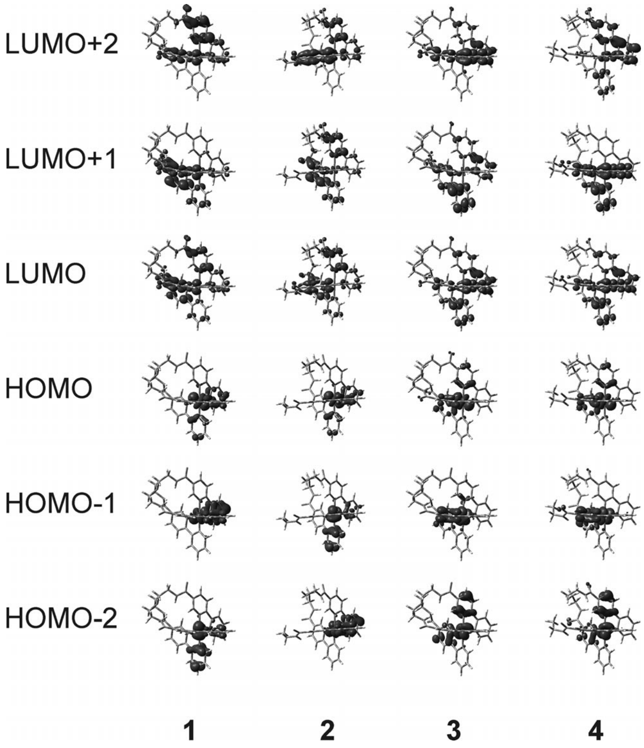

Figure 4. Isodensity surface plots of some selected frontier molecular orbitals for complexes **1**–**4** at their optimized S_0 geometry in the gas phase. Isodensity value: 0.035 e Bohr^{-3}. A larger version is given in Figures S4–S6 of the Supporting Information).

Table 1. List of selected molecular orbital energies [eV] for complexes **1**–**4** and *fac*-[Ir(ppy)$_3$] at their S_0-optimized geometry in vacuo, and HOMO–LUMO energy gap.

Orbital	*fac*-[Ir(ppy)$_3$]	**1**	**2**	**3**	**4**
LUMO + 4 (e)	–0.653	–1.192	–1.169	–1.054	–1.082
LUMO + 3 (a)	–0.894	–1.501	–1.337	–1.277	–1.306
LUMO + 2 (e)	–1.131	–1.758	–1.719	–1.620	–1.630
LUMO + 1 (e)	–1.131	–1.758	–1.719	–1.620	–1.630
LUMO (a)	–1.221	–1.844	–1.842	–1.728	–1.763
HOMO (a)	–4.881	–5.268	–5.261	–5.352	–5.384
HOMO – 1 (e)	–5.018	–5.314	–5.389	–5.382	–5.394
HOMO – 2 (e)	–5.018	–5.314	–5.389	–5.382	–5.394
HOMO – 3 (e)	–5.862	–6.165	–6.215	–6.207	–6.213[a]
HOMO – 4 (e)	–5.862	–6.165	–6.215	–6.207	–6.221
HOMO–LUMO gap	3.661	3.424	3.419	3.624	3.620

[a] "a" symmetry.

The three HOMOs mainly correspond to the 5d orbitals of the d^6 Ir^{III} center in a (distorted) octahedral environment, and are denoted d$_{1a}$, d$_{1b}$, and d$_2$, for which d$_{1a}$ and d$_{1b}$ are the twofold degenerated orbitals with "e" symmetry, and d$_2$ is the highest energy orbital with "a" symmetry. Nonetheless, a sizeable admixing between the three filled d orbitals of the iridium and the π-orbitals of the ligand can be clearly envisaged, as is typical of cyclometalated iridium(III) complexes. In particular, the HOMO (namely, d$_2$) is an antibonding combination of Ir(t$_{2g}$) and π orbitals of two of the cyclometalating phenyl rings of A symmetry. The corresponding energy was calculated to be –5.268, –5.261, –5.352, and –5.384 eV for complex **1**, **2**, **3**, and **4**, respectively. It is worth noting that in both couples of complexes the presence of the capping unit causes a negligible difference in the HOMO energy level. On the other hand, due to the nature of the HOMO, the position of the amido substituent (phenyl versus pyridyl ring) has a larger influence on the stabilization of the orbital. Complex **4** is stabilized by as much as 0.123 eV with respect to complex **2**. At slightly more negative energies, two degenerate d$_{1a}$ and d$_{1b}$, namely, HOMO – 1 and HOMO – 2, are encountered. Their nature can be mainly described as the two antibonding combinations of the Ir(t$_{2g}$) and the π orbitals of two of the cyclometalating phenyl rings of E symmetry. These orbitals are stabilized with respect to the corresponding HOMO level by 0.046, 0.128, 0.029, and 0.01 eV, and lie at –5.314, –5.389, –5.382, and –5.394 eV, for **1**, **2**, **3**, and **4**, respectively. Going from the occupied to the virtual molecular orbitals, the three lowest-lying unoccupied molecular orbitals can be denoted, in order of increasing energy, as π*$_1$, π*$_{2a}$, and π*$_{2b}$. The LUMO, namely, π*$_1$, can be described as the combination π* orbitals of the ligands of "a" symmetry, mainly localized on the pyridyl rings, and extends over the carbonyl group of the amido substituents in complexes **1** and **2**. Such an orbital is calculated to lie at –1.844, –1.842, –1.728, and –1.763 eV for **1**, **2**, **3**, and **4**, respectively. As far as complexes **1** and **2** are concerned, the presence of the electron-withdrawing amido groups, which are strongly involved in the LUMO, induces a stabilization of the corresponding energy level with respect to the *fac*-[Ir(ppy)$_3$] as high as 0.623 and 0.621 eV, for **1** and **2**, respectively. On the other hand, such a stabilization effect is lower for complexes **3** and **4**, with values of 0.507 and 0.542 eV, respectively. Finally, a set of twofold degenerate orbitals of "e" symmetry lies at –1.758 (**1**), –1.719 (**2**), –1.620 (**3**), and –1.630 eV (**4**), which can be described as the combination of π* of the pyridyl moieties, and extends over the carbonyl group of the amido substituents in complexes **1** and **2**.

The UV/Vis absorption spectra of both pairs of hemicage and open complexes are reported in Figure 5, and the typical absorption maxima and shoulder are reported in Table 2 together with their molar extinction coefficients. Also, to gain deeper insight into the nature of the electronic transition involved in the absorption spectra, complexes **1**–**4** were investigated by means of time-dependent density functional theory (TD-DFT) calculations, and the computed vertical transitions described in terms of molecular orbitals of the corresponding ground-state geometry. The most relevant lowest-lying singlet-to-singlet ($S_0 \rightarrow S_n$, n = 1–30) and the three lowest-lying singlet-to-triplet ($S_0 \rightarrow T_n$, n = 1–3) calculated transitions are respectively listed in the Supporting Information together with the nature of the involved orbitals and their expansion coefficients (see Tables S7 and S8). In the experimental spectra, all the complexes show a strong absorption band ($\varepsilon \geq 10^4$ $\mathrm{M^{-1}\,cm^{-1}}$) between 280 and 320 nm and weaker absorption bands ($\varepsilon \leq 10^3$ $\mathrm{M^{-1}\,cm^{-1}}$) between 350 and 450 nm. By comparison with the typical absorption shown by *fac*-[Ir(ppy)$_3$] derivatives,[27,28] the absorption bands centered around 300 nm can be assigned to ligand-centered $\pi \rightarrow \pi^*$ transitions, whereas the weaker bands centered around 400 nm can be assigned to the convolution of the lowest-lying spin-allowed singlet-to-singlet metal-to-ligand charge transfers (^{1}MLCTs). It is worth noting that the hemicaged complex **1** showed a slight bathochromic shift of its MLCT absorption bands compared to the open complex **2**, whereas no similar shift was observed for derivatives **3** and **4**. These findings nicely agree with the TD-DFT calculations. In particular, the lowest-energy transitions are the $S_0 \rightarrow S_1$ and mainly involve the iridium d orbitals (partially mixed with the π orbitals of the cyclometalating phenyl rings) and π* orbitals of the pyridyl moieties (HOMO → LUMO, ^{1}MLCT$_1$), and are computed to lie at 450, 453, 427, and 429 nm for complex **1**, **2**, **3**, and **4**, respectively. At slightly higher energies, two doubly generated ^{1}MLCT transitions with moderate oscillator strengths (f = 0.018–0.047) were computed, which can be ascribed to linear combinations of HOMO – 1/HOMO – 2 → LUMO (^{1}MLCT$_2$, with E symmetry) and HOMO – 1/HOMO – 2 → LUMO + 1/LUMO + 2 (^{1}MLCT$_3$, with A symmetry). Such transitions are calculated to occur at 435 and 423 nm (**1**); 425 and 410 nm (**2**); 414 and 399 nm (**3**); and 418 and 398 nm (**4**), respectively. At higher energies, such transitions are followed by A-symmetry excitation with intensities similar to the above-described processes and involve HOMO → LUMO + 3 (computed at 399 and 379 nm, for **1** and **2**, respectively) and linear combination of HOMO – 1/HOMO – 2 → LUMO + 1/LUMO + 2 (computed at 389 and 388 nm, for **3** and **4**, respectively). Moreover, the weak shoulder at lower energies (centered around 470 nm) can be assigned to spin-forbidden singlet-to-triplet ^{3}MLCT. The latter transitions are usually observed in complexes that contain heavy atoms (like iridium), which show a remarkable spin–orbit coupling that makes the singlet-to-triplet transitions partially allowed. Such transitions are in very good agreement with the theoretical ($S_0 \rightarrow T_1$) excitation energies, which are computed to be 502, 498, 485, and 486 nm, for **1**, **2**, **3**, and **4**, respectively.

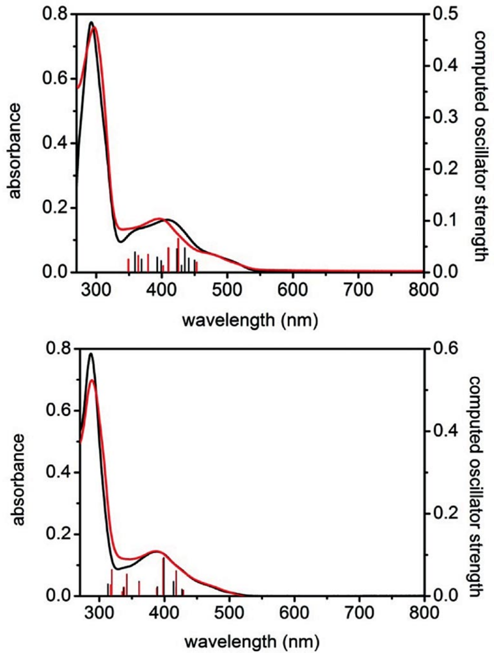

Figure 5. UV/Vis absorption of **1** (black), **2** (red) (top), and **3** (black), and **4** (red) (bottom) in DMF at room temp., and corresponding lower-lying computed excitation energies and oscillator strengths (vertical lines).

Table 2. UV/Vis absorption data of **1**–**4** and their molar extinction coefficient in DMF at room temp.

	Absorption[a] λ [nm], (ε [10^3 $\mathrm{M^{-1}\,cm^{-1}}$])
1	292 (45), 302 (sh. 15), 361 (sh. 5.3),420 (6.5), 487 (sh. 2.1)
2	297 (32), 400 (6.9), 487 (sh. 2.1)
3	287 (52), 387 (9.4), 474 (sh. 2.1)
4*	288 (45), 387 (6.3), 474 (sh. 2.6)

[a] sh. = shoulder; * = estimated value because of the poor solubility of **4** in DMF.

All the reported complexes **1**–**4** showed intense luminescence at room temperature (Figure 6). As expected, the presence of electron-withdrawing groups on the pyridine ring induced a bathochromic shift in the emission of complexes **1** and **2** compared to the archetypical *fac*-[Ir(ppy)$_3$] as a consequence of the stabilization of the LUMO orbital. Conversely, the same groups on the phenyl ring minimally stabilize the HOMO orbital to result in a slight redshift of the emission of the complexes **3** and **4** compared to [Ir(ppy)$_3$].[1] This different effect between **1** and **2** on the one hand and **3** and **4** on the other is due to the low atomic contribution given to the HOMO orbital by the atom on which the amide moiety is located.[29] The hemicaged complex **1** showed an evident redshift of the emission compared to the open complex **2**. Conversely, the hemicaged complex **3** showed a slight ipsochromic shift of the emission compared to the open complex **4**. As already mentioned, the rigidity and lack of flexibility induced by the capping unit blocks the rotation of the amido group, which is almost coplanar with the pyridine ring (see Table S7 in the Supporting Information).[17] Furthermore, the locally different polarity induced by the presence of the N atom of the capping unit can influence the degree of shift (e.g., a kind of local solvatochromism).[30] The situation is different when the phenyl is substituted with the amido group, since a destabilization of the HOMO orbital is expected. The slight blueshift observed for the hemicage **3** with respect to **4** can again be explained by the structural rigidity induced by the capping and by the locally different polarity induced by the presence of the N atom of the capping unit.[30] The increase in energy for the HOMO–LUMO gap in the phenyl-substituted complexes **3** and **4** implies that the lowest excited state, ^{3}MLCT, is more mixed with the ^{3}LC energetically accessible, as can be seen by the structured emission and longer excited-state lifetimes. On the other hand, the structureless emission bands shown by complexes **1** and **2** indicate that the excited state of those complexes has mainly an ^{3}MLCT character.[27]

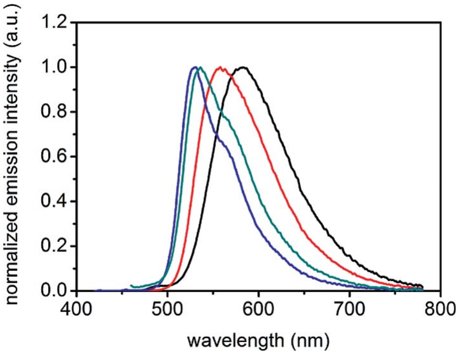

Figure 6. Normalized emission profile of **1** (black), **2** (red), **3** (blue), and **4** (green) in DMF at room temperature and upon excitation at λ = 400 nm.

The photophysical properties of **1**–**4** are summarized in Table 3; all complexes were highly luminescent in oxygen-free solvents, with quantum yields Φ_0 of 0.54 up to 0.81. Long excited-state lifetimes (τ_0 = 1.0–1.7 µs) were observed for all the complexes, thereby confirming the triplet nature of the emission. In air-equilibrated solutions, a general decrease of quantum yields and lifetimes was observed as a consequence of the oxygen quenching. Under these conditions, the hemicaged **1** showed a higher quantum yield (Φ = 0.048) than the open form **2** (Φ = 0.040), whereas complexes **3** and **4** show basically the same quantum yield (Φ = 0.035 and 0.034, respectively). The same trend was observed for the emission lifetimes in deaerated solution. The hemicage **1** showed a longer lifetime (τ = 100 ns) than the open complex **2** (τ = 78 ns), whereas the two complexes substituted on the phenyl ring showed practically the same lifetime (τ = 78 and 77 ns for **3** and **4**, respectively). The different trend observed for the quantum yields and excited-state lifetimes of the hemicaged **1** and the open form **2** in the absence and presence of oxygen provides a first indication of the different behavior towards oxygen quenching. In contrast, a quite similar decrease is observed for the two complexes **3** and **4**, which suggests a comparable behavior of these two compounds towards oxygen quenching. Therefore, comparison of the two pairs of complexes shielded on the pyridine (**1**, **2**) or on the phenyl (**3**, **4**) ring provides an explanation for the different oxygen sensitivity, which is induced by the shielding of the atoms on which the LUMO (**1**, **2**) or the HOMO (**3**, **4**) orbitals are localized. According to these qualitative data, the shielding of the LUMO exerts an important effect on the oxygen sensitivity, whereas the shielding of the HOMO does not have any relevant effect. A more quantitative evaluation of the difference in oxygen quenching was obtained by a Stern–Volmer analysis of the luminescence quenching (vide infra).

Table 3. Photophysical properties of hemicaged and open complexes in DMF at 25 °C (unless stated).[a]

	λ_{em} [nm]	ϕ_0		τ_0 [ns]	τ [ns]	λ_{em} [nm] (77 K)[a]	τ [µs] (77 K)[a]
1	580	0.54	0.048	1013	100	540	5.56
2	556	0.62	0.040	1110	78	532	5.06
3	532	0.81	0.035	1775	78	521	5.03
4	537	0.63	0.034	1620	77	519	4.68

[a] Measured in CH_2Cl_2/MeOH (1:1) glass. Values of ϕ_0 and ϕ are quantum yields in degassed and aerated solutions, respectively; τ_0 and τ are lifetimes in degassed and aerated solutions, respectively.

The emission spectra obtained in rigid matrices at 77 K (Figure 7) show that all the compounds **1**–**4** undergo a blueshift of the emission maximum with respect to the room-temperature emission. This observation confirms that there is a ^{3}MLCT character of the emitting state.[31] The long lifetime recorded at 77 K for all the complexes and the structure of the emission again indicate the mixing with the ^{3}LC states and the triplet character of the emitting state.

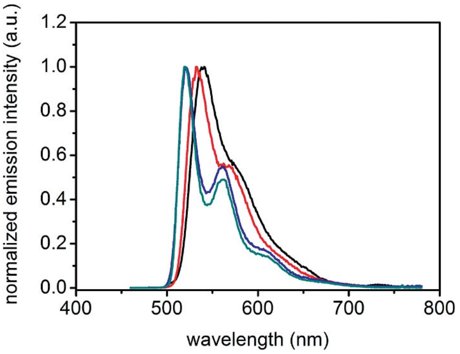

Figure 7. Normalized emission profile of **1** (black), **2** (red), **3** (blue), and **4** (green) in CH_2Cl_2/MeOH (1:1) glass at 77 K upon excitation at λ = 400 nm.

All the relevant electrochemical data are summarized in Table 4. For complex **1**, the main aspect that emerges from the electrochemical analysis is the effect played by the hemicage formation on lowering the LUMO level of **1** by about 0.1 eV compared to **2**. The presence of the hemicage seems to induce a more effective conjugation (coplanarity) of the amide bond in the *meta* position in the pyridyl moiety of **1** compared to that in **2**, thus stabilizing the LUMO. In fact, **1** is more easily reduced than its related open-form **2** ($E^{o}_{red,1} > E^{o}_{red,2}$). This finding could also be ascribed to a sizeable difference in solvation between **1** and **2**, but such stabilization is not evidenced by DFT calculations even if the solvation effect is taken into account by means of a conductor-like polarizable continuum model (PCM) as single-point calculation at the S_0-optimized geometry (see Table S11 in the Supporting Information). However, while comparing theoretical and electrochemical HOMO and LUMO energy levels, one should keep in mind that calculated values are approximations of the ionization potential (HOMO) and electron affinity (LUMO) (i.e., vertical oxidation and reduction potentials), whereas the electrochemical values are the result of adiabatic (equilibrium) processes, which lead to the formation of radical cation and anion, respectively. The HOMO level is not affected by the hemicage structure ($E^{o}_{ox,1} \approx E^{o}_{ox,2}$), which confirms that it is mainly centered on the Ir metal core, as also supported by DFT calculations (vide supra).

Table 4. Electrochemical potential values (versus SCE) for samples **1**–**4** in DMF/0.1 M tetrabutylammonium hydroxide (TBAH).[a][b][c]

	E^{o}_{red} [LUMO]	E^{o}_{ox} [HOMO]	ΔE_{H-L}
1	–1.74 V, r [–2.60 eV]	+0.92 V, r [–5.26 eV]	2.66 eV
2	–1.87 V, r [–2.46 eV]	+0.91 V, r [–5.25 eV]	2.78 eV
3	–1.78 V, r [–2.56 eV]	+1.06 V [–5.40 eV]	2.84 eV
4	n/a[d]	n/a[d]	n/a[d]

[a] The sample solutions under investigation were 1 mM in DMF/0.1 M TBAH. A glassy carbon was employed as the working electrode, a platinum ring as the counter, and a silver wire as the reference. The scan rate was varied in the range of 0.2–5 V s^{-1}. $E = E^{o}$ calculated as the mean value between the cathodic and the anodic peak averaged in the scan rate range 0.2–0.5 V s^{-1}. [b] The peak-to-peak separation was ranging between 70 and 80 mV at 0.2 V s^{-1}, which is larger than expected for an ideal Nernstian behavior (59 mV). However, the behavior of the redox couple ferrocene/ferricenium ($Fc^{+}|Fc^{0}$), used as internal standard, showed the same trend. Therefore, we can attribute the observed effect to the ohmic drop of the system, as previously reported for aprotic media by Bard and co-workers.[47] The peak currents instead were found to be linearly dependent on the square root of the scan rate as expected for a diffusion-controlled redox process. [c] Reversible peak. [d] The solubility of **4** was poor under these experimental conditions, and it was not possible to estimate the potential values.

Furthermore, by comparison of **1** and **3**, the reduction potentials (E^{o}_{red}) of these two hemicaged systems differ by about 40 mV. The presence of the amide bond in the *meta* position in the pyridyl moiety is more effective in stabilizing the LUMO than in the phenyl moiety of **3**, thus corroborating the evidence of the redshift observed in the emission spectra (vide supra). Compound **4** is poorly soluble under the conditions used for the electrochemical measurements, and it was not possible to estimate the HOMO and LUMO values from electrochemical measurements. Nevertheless, because of the similar photophysical characteristics of **3** and **4**, it is possible to make an educated guess also for **4** (vide infra).

The luminescence oxygen quenching processes of complexes **1**–**4** were studied by monitoring the luminescence intensity of solutions with different concentrations of oxygen and by plotting the obtained results according to the Stern–Volmer equation [Equation (1)].

$$\frac{I_0}{I} = 1 + k_q \tau_0 [O_2] \qquad (1)$$

for which I_0 and I are the emission intensities in the absence or presence of quencher, respectively, k_q is the quenching constant, τ_0 is the lifetime in the absence of quencher, and $[O_2]$ the concentration of oxygen in solution.[32] The Stern–Volmer plots for the four complexes are reported in Figure 8.

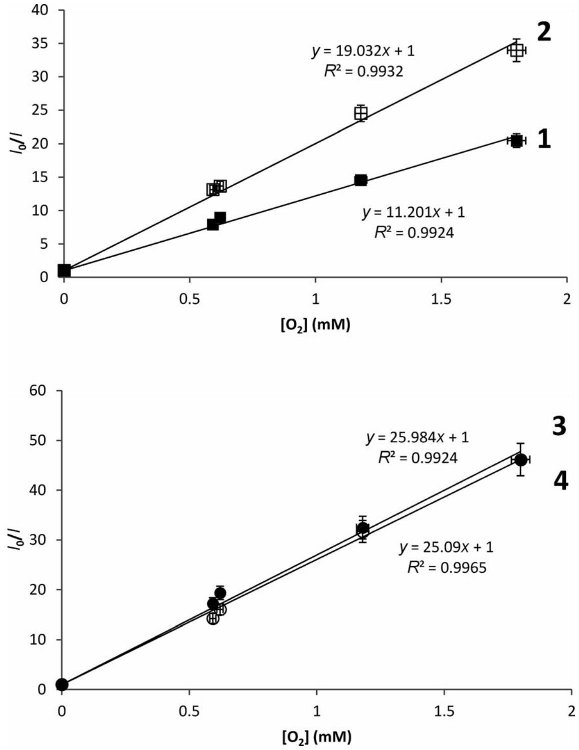

Figure 8. Stern–Volmer plot of complexes **1**–**4** in DMF at room temperature. Comparison of the oxygen quenching of the two couples of complexes shows that introduction of a capping unit on the pyridine side (hemicaged **1**) induces a decrease in oxygen quenching with respect to the open form **2**. Conversely, only a minor difference is observed between **3** and **4**, functionalized on the phenyl side.

The quenching constant k_q was calculated according to Equation (1) from the value of the slope obtained by fitting the Stern–Volmer plot. By consecutive comparison of the quenching constants (Table 5), it was possible to determine the efficiency of oxygen quenching. The pyridine-substituted complexes showed a remarkable decrease in oxygen quenching (40 %) going from the open (**2**) to the hemicaged (**1**) complex, whereas no noticeable changes were observed in the case of the phenyl-substituted complexes (**3**, **4**). To exclude any difference in terms of energy or electron trans-

Table 5. Oxygen quenching constant (k_q) and thermodynamic parameters involved in the oxygen quenching mechanisms.

	E_{00} [eV]	ΔG_{et} [kJ mol^{-1}] [a]	ΔG_{el} [kJ mol^{-1}]	k_q [M^{-1} s^{-1}])
1	2.42	–139	–69	1.0×10^{10}
2	2.43	–140	–71	1.7×10^{10}
3	2.47	–144	–60	1.5×10^{10}
4	2.47	–144	–	1.6×10^{10}
IrCage[b]	–	–	–	0.5×10^{10}
$[Ir(ppy)_3]$[c]	2.52	–149	–95	2.4×10^{10}[b]

[a] Calculated assuming $E_{O_2^*}(^1\Delta_g)$ = 0.98 eV. [b] From the literature.[18] [c] Calculated on the basis of the photophysical data from the literature[21] unless otherwise stated.

fer, the free energies of energy transfer (ΔG_{et}) and of electron transfer (ΔG_{el}) were calculated according to Equations (2) and (3).

$$\Delta G_{et} = -(E_{00} - E_{O_2*}) \tag{2}$$

$$\Delta G_{el} = F(E_F^{ox} - E_{O_2}^{red}) - E_{00} + C \tag{3}$$

E_{00} is the energy of the 0–0 transition and $E_{\mathrm{O_2}*}$ the energy of the excited state of singlet oxygen: $E_{\mathrm{O_2}*}(^1\Sigma_g)$ = 1.63 eV and $E_{\mathrm{O_2}*}(^1\Delta_g)$ = 0.98 eV depending on which excited state of oxygen is initially produced during quenching, F is Faraday's constant, $E_{\mathrm{F}}^{\mathrm{ox}}$ is the oxidation potential of the fluorophore, $E_{\mathrm{O_2}}^{\mathrm{red}}$ is the reduction potential of oxygen (–0.78 V), and C is a Coulomb term (usually neglected in polar solvents).[33–35] The calculated values of ΔG_{et} and ΔG_{el} are reported in Table 5. The evaluation of the ΔG_{el} of the open complex **4** was not possible because of its low solubility in DMF, which precludes the possibility of recording the potentiometric data. However, since both k_{q} and ΔG_{et} appeared to be identical for **3** and **4** within the experimental error, it is reasonable to assume that also ΔG_{el} will have the same value for both compounds. From the analysis of these data, it is possible to conclude that both the hemicaged and open molecule of each pair show only a modest difference in terms of thermodynamic feasibility of energy or electron transfer. The basically equal thermodynamic feasibility of energy and electron transfer between the pair of complexes **1**, **2** and **3**, **4** suggests that the remarkable difference observed in the quenching constant k_{q} between the hemicaged (**1**) and the open (**2**) complex functionalized on the pyridine side of the [Ir(ppy)$_3$] is due to a structural effect.

The caged complex (**ii**, Scheme 1) previously reported by our group shows a further 50% decrease in the oxygen quenching ($k_{\mathrm{q}} = 0.5\times10^{10}$ M^{-1} s^{-1}) with respect to **1**.[18] On the basis of the emission maximum (λ_{em} = 570 nm), it is reasonable to hypothesize that the energy of the triplet state (E_{00}) of the cage has likely an intermediate value between the E_{00} of **1** (λ_{em} = 580 nm) and **2** (λ_{em} = 556 nm), therefore the value of the free energy of the energy transfer ΔG_{et} can be estimated to be similar to the ΔG_{et} of **1** and **2**. On the other hand, because of the presence of two amide moieties on the phenylpyridine ligands, the oxidation potential of the cage is probably higher than the oxidation potential of **1**.[1] Consequently, the value of the free energy of the electron transfer ΔG_{el} is probably higher than the value found for **1**, thereby resulting in a less favorable thermodynamic feasibility of electron transfer. In conclusion, on the basis of the estimated thermodynamic parameters, it is possible to hypothesize that the low degree of oxygen quenching observed for the caged complex **ii** probably derives from a decreased thermodynamic feasibility of the electron transfer with respect to **1**. We believe, however, that structural factors also play an important role in the low degree of oxygen quenching of the caged Ir$^{\mathrm{III}}$ complex **ii**: it has been observed that in the caged complex the amide moiety located on the pyridine side shows the carbonyl oriented towards the inner side of the molecule. According to computational models, in the hemicaged complexes **1** and **2** the LUMO orbital is partly localized on the carbonyl moiety (vide supra). Therefore, the orientation of the pyridine carbonyl towards the inner side of the cage would likely result in a higher degree of LUMO shielding and a consequent decrease in the oxygen quenching degree, since the lowest excited state is an MLCT in which the ligand involved is indeed the pyridine unit.

Conclusion

We have reported the synthesis, characterization, and photochemical properties of two pairs of iridium(III)–tris(phenylpyridine) derivatives with a hemicaged (**1**, **3**) or open (**2**, **4**) structure. The results obtained from this systematic study of the oxygen quenching of hemicages and open complexes shielded on the pyridine (**1**, **2**) or on the phenyl (**3**, **4**) ring show the hemicaged complex that bears a capping unit on the pyridine ring (**1**) to have a much lower oxygen quenching constant ($k_{\mathrm{q}} = 1.0\times10^{10}$ M^{-1} s^{-1}) than its parent open complex **2** with ethylamide on the pyridine rings ($k_{\mathrm{q}} = 1.7\times10^{10}$ M^{-1} s^{-1}). Moreover, the hemicaged complex **3**, in which the capping unit is connected to the phenyl rings, shows basically the same degree of oxygen quenching as the open complex **4** functionalized with ethylamides on the phenyl rings ($k_{\mathrm{q}} = 1.5\times10^{10}$ and 1.6×10^{10} M^{-1} s^{-1}, respectively). The ΔG_{et} and ΔG_{el} parameters show that in terms of thermodynamic feasibility only a modest difference exists between the members of each pair of compounds (**1**, **2** and **3**, **4**) and, therefore, the lower quenching shown by **1** with respect to **2** can be ascribed to a structural effect. The structural (shielding) effect induced by the presence of the capping unit is due to the shielding of the LUMO orbital exerted by the capping unit, which is possibly enforced by the high degree of twisting of the hemicaged complex **1**. It is reasonable to hypothesize that both these parameters give a contribution that results in a lower degree of oxygen quenching of **1** with respect to **2**, but on the basis of the structural and photophysical data available it was not possible to quantify the respective contributions of the two effects. The introduction of a capping unit on the phenyl ring induced only a minor change in the oxygen sensitivity of the hemicaged complex **3** with respect to the open complex **4**, which is explained by the fact that the LUMO of the hemicage **3** is mostly localized on the pyridine ring, and the luminescent state is an MLCT that involves the pyridine. The structure–photoluminescence quenching relationship obtained from this study together with thermodynamic considerations for the substituents on the phenylpyridine ring nicely explain the observed shielding mechanism in the hitherto only reported iridium(III) caged complex.

Experimental Section

General: The NMR spectroscopic experiments were performed with a Bruker Avance II NMR spectrometer operating at 600.35 MHz for ^{1}H and 150.09 MHz for ^{13}C. Chemical shifts are given in ppm using the residual solvent signal as reference. The multiplicity of the peaks is reported by using the following abbreviations: s = singlet, d = doublet, t = triplet, quint = quintuplet, m = multiplet. The chemical shifts and assignments of ^{13}C signals are reported in the Supporting Information. Mass spectra were measured with a Micromass LCT (ESI-HRMS) spectrometer. IR spectra were measured with a Thermo Scientific Nicolet 6700 FTIR spectrometer equipped with a Smart Orbit diamond ATR accessory. Main bands are reported and assigned to functional groups by using the following abbreviations: br. = broad band, str. = stretching band, def. = deformation band. UV/Vis spectra were measured with a Perkin–Elmer Lambda 850 UV/Vis spectrophotometer by using a quartz cuvette with 1 cm path length. Steady-state luminescence spectra were measured with an Edinburgh FS900 fluorospectrometer. A 450 W xenon arc lamp was used as excitation source. Luminescence quantum yields at room temperature (Φ and Φ_{air}) were evaluated by comparing wavelength-integrated intensities (I) of isoabsorptive optically diluted solutions (abs. < 0.1) with reference to $[Ru(bpy)_3]Cl_2$ ($\Phi_R = 0.028$ in air-equilibrated water) or fluorescein ($\Phi_R = 0.95$ in 0.1 M NaOH) standard for the complexes **1**, **2** and **3**, **4**, respectively, and by using the Equation (4), in which n and n_R are the refractive index of the sample and reference solvent, respectively.[36]

$$\Phi = \Phi_R \frac{n^2 I}{n_R^2 I_R} \tag{4}$$

Luminescence lifetimes of the compounds were determined by recording the decay curves of the luminescence intensity at the emission maximum using the TCSPC option on a HORIBA Jobin Yvon Fluoromax 4 instrument and a pulsed solid-state LED as excitation source at 462 nm wavelength. The recorded data were analyzed using the DAS6 software package of HORIBA Jobin Yvon. Degassed solutions were prepared by four freeze–pump–thaw cycles. Electrochemical measurements were done in *N*,*N*-dimethylformamide (Acros, extra dry over molecular sieves, 99.8%), which was used as received without any further purification. Tetrabutylammonium hexafluorophosphate (electrochemical grade, ≥99%, Fluka) was used as supporting electrolyte, which was recrystallized from a 1:1 ethanol/water solution and dried at 60 °C under vacuum. For the electrochemical experiments, a CHI750C Electrochemical Workstation (CH Instruments, Inc., Astin, TX, USA) was used. The electrochemical experiments were performed in a glass cell under an Ar atmosphere. To minimize the ohmic drop between the working and the reference electrodes, feedback correction was employed. The electrochemical experiments were performed by using a 3 mm diameter glassy carbon disk electrode (homemade from Tokai glassy carbon rod). Before the experiments, the working electrode was polished with a 0.05 µm diamond suspension (Metadi Supreme Diamond Suspension, Buehler) and ultrasonically rinsed with ethanol for 5 min. The electrode was electrochemically activated in the background solution by means of several voltammetric cycles at 0.5 V s^{-1} between the anodic and cathodic solvent/electrolyte discharges until the same quality features were obtained. The reference electrode was a silver quasi-reference electrode (AgQRE), which was separated from the catholyte by a glass frit (Vycor). The reference electrode was calibrated at the end of each experiment against the ferrocene/ferricenium couple, the formal potential of which in *N*,*N*-dimethylformamide is 0.464 V against the standard calomel electrode (SCE) with satd. aqueous KCl; all potential values are reported against SCE. A platinum ring or coil served as the counter electrode.

Solutions with different oxygen concentration, suitable for the Stern–Volmer quenching studies, were prepared by using N_2/O_2 mixtures prepared with a Brooks 5850S Mass Flow control and by purging the fluorophore solutions for 40 min.

Computational Details: Geometries were optimized by means of DFT and employing the exchange correlation hybrid functional B3LYP.[15,37,38] The standard valence double-ζ polarized basis set 6-31G(d,p)[39] was used for C, H, N, and O. For Ir, the Stuttgart–Dresden (SDD) effective core potentials were employed along with the corresponding valence triple-ζ basis set. All the calculations were done assuming C_3 symmetry. The nature of all the stationary points was checked by computing vibrational frequencies, and all the species were found to be true potential energy minima, as no imaginary frequency was obtained ($N_{Imag} = 0$). Single-point calculations at the S_0-optimized geometry were done also in the solvent used for the electrochemical characterization (*N*,*N*-dimethylformamide), described by means of a conductor-like polarizable continuum model (PCM).[40–42]

To simulate the absorption electronic spectrum down to 300 nm, for each complex the lowest 30 singlet ($S_0 \rightarrow S_n$) as well as the four lowest triplet excitation energies ($S_0 \rightarrow T_n$) were computed on the optimized geometry at the S_0 by means of TD-DFT calculations.[43,44] Oscillator strengths were deduced from the dipole transition-matrix elements (for single states only). Isodensity surfaces plots of selected orbitals for the investigated structures in the gas phase at their optimized ground-state geometry were plotted at isodensity value of 0.035 e Bohr^{-3}. All the calculations were performed with Gaussian 09 program package.[45]

Materials: Oxygen-sensitive reactions were carried out by using standard Schlenk techniques. Commercial-grade reagents were purchased from Sigma–Aldrich and used without further purification. 4-(Pyridin-2-yl)benzoic acid (**8**) was prepared according to the literature procedure.[46]

6-Phenylnicotinic Acid (5): Phenylboronic acid (3 g, 24.6 mmol), 6-bromonicotinic acid (3.66 g, 18.2 mmol), and tetrakis(triphenylphosphane)palladium(0) (900 mg, 0.78 mmol) were dissolved in a mixture (180 mL) of Na_2CO_3 (0.2 M) and acetonitrile (1:1). After several argon/vacuum cycles, the reaction was heated at reflux for 48 h. The hot reaction mixture was filtered through Celite, the acetonitrile removed, and the resulting aqueous solution was extracted several times with CH_2Cl_2. The aqueous solution was then acidified with acetic acid and the white precipitate was filtered and dried with P_2O_5; yield 3.1 g (15.6 mmol; 85%) of pure compound. ^1H NMR ([D$_6$]DMSO): $\delta = 9.15$ (s, 1 H), 8.33 (d, $J = 12$ Hz, 1 H), 8.15 (d, $J = 6$ Hz, 2 H), 8.10 (d, $J = 12$ Hz, 1 H), 7.54–7.49 (m, 3 H) ppm. ^{13}C NMR ([D$_6$]DMSO): see the Supporting Information. IR (neat): $\tilde{\nu} = 1673$ (C=O str.), 1417 (OH def. acid), 935 (OH def. acid) cm^{-1}. ESI-HRMS: calcd. for $C_{12}H_9NO_2$ 199.063 [M$^+$]; found 199.065.

General Synthesis of Hemicaged Ligands: Acid (600 mg, 3 mmol), *N*,*N*′-dicyclohexylcarbodiimide (620 mg, 3 mmol), and *N*-hydroxybenzotriazole (400 mg, 3 mmol) were dissolved in dry *N*,*N*′-dimethylacetamide (50 mL). Tris(2-aminoethyl)amine (120 µL, 0.8 mmol) was added dropwise and the resulting mixture was stirred overnight at 60 °C. The reaction mixture was then filtered and added to ethyl ether (ca. 400 mL) under vigorous stirring. The white precipitate was then collected by filtration and washed with hot acetonitrile. In a typical experiment, 212 mg (0.3 mmol, 40%) of pure tripodal ligand was obtained.

Hemicaged Ligand (6): ^1H NMR ([D$_4$]MeOH): $\delta = 8.90$ (s, 1 H), 7.93 (dd, $J = 12$ Hz, 1 H), 7.73 (d, $J = 6$ Hz, 2 H), 7.43 (d, $J = 6$ Hz, 1 H), 7.37 (t, $J = 6$ Hz, 1 H), 7.29 (t, $J = 6$ Hz, 2 H), 3.60 (t, $J = 6$ Hz, 2 H), 2.82 (t, $J = 6$ Hz, 2 H) ppm. ^{13}C NMR ([D$_4$]-

MeOH): see the Supporting Information. IR (neat): ṽ = 3396 (NH str.), 2948 (CH$_2$ str.), 2815 (N–CH$_2$/CH$_2$ str.), 1630 (C=O str.), 1587 (NH bend.), 1465 (CH$_2$–N str.), 743 (N–C–O str.) cm^{-1}. ESI-HRMS: calcd. 690.319 [M + H$^+$]; found 690.320.

Hemicaged Ligand (9): ^{1}H NMR ([D$_4$]MeOH): δ = 8.46 (s, 1 H), 7.69 (d, J = 6 Hz, 2 H), 7.66 (d, J = 6 Hz, 2 H), 7.59 (t, J = 12 Hz, 1 H), 7.49 (d, J = 6 Hz, 1 H), 7.24 (t, J = 6 Hz, 1 H), 3.59 (t, J = 6 Hz, 2 H), 2.82 (t, J = 6 Hz, 2 H) ppm. ^{13}C NMR ([D$_4$]MeOH): see the Supporting Information. IR (neat): ṽ = 3293 (NH str.), 3055 (CH$_2$ str.), 2925 (CH$_2$ str.), 2790 (N–CH$_2$/CH$_2$ str.), 1631 (C=O str.), 1537 (NH bend.), 1463 (CH$_2$–N str.), 752 (N–C–O str.) cm^{-1}. HRMS: calcd. 690.319 [M + H$^+$]; found 690.317.

General Synthesis of Ethylamide Ligands: Acid (1 g, 5 mmol) and 1-ethyl-3-[3-(dimethylamino)propyl]carbodiimide (1.9 g, 12.5 mmol) were dissolved in a mixture (60 mL) of CH$_2$Cl$_2$/pyridine (7:3). Ethylamine (3 mL, 2.0 M in THF) was added dropwise, and the mixture was stirred dropwise at room temperature. The solvent was removed under vacuum, and the crude was then suspended in water and extracted with ethyl acetate. The organic phase was washed with a satd. solution of CuSO$_4$, then with satd. NH$_4$Cl, and eventually with brine. The organic phase was then dried with Na$_2$SO$_4$ and the solvent removed by rotavapor. Typically, 1 g (4.25 mmol; 85%) of pure compound was obtained.

***N*-Ethyl-6-phenylnicotinamide (7):** ^{1}H NMR ([D$_6$]DMSO): δ = 9.21 (s, 1 H), 8.38 (d, J = 6 Hz, 1 H), 8.21 (d, J = 6 Hz, 2 H), 8.13 (d, J = 6 Hz, 1 H), 7.57–7.50 (m, 3 H), 3.43 (q, J = 6 Hz, 2 H), 1.21 (t, J = 6 Hz, 3 H) ppm. ^{13}C NMR ([D$_4$]MeOH): see the Supporting Information. IR (neat): ṽ = 3322 (N–H str.), 2975 (CH$_3$ str.), 2931 (CH$_2$ str.), 2877 (CH$_3$ str.), 1627 (C=O str.), 1522 (N–H str.), 1469 (CH$_2$–N str.), 1267 (CH$_3$ str.), 746 (N–C–O str.) cm^{-1}. ESI-HRMS: calcd. 226.111 [M$^+$]; found 226.113.

***N*-Ethyl-4-(pyridin-2-yl)benzamide (10):** ^{1}H NMR ([D$_6$]DMSO): δ = 8.71 (d, J = 6 Hz, 1 H), 8.57 (t, J = 6 Hz, 1 H), 8.18 (d, J = 6 Hz, 2 H), 8.05 (d, J = 6 Hz, 1 H), 7.96 (d, J = 6 Hz, 2 H), 7.94 (t, J = 12 Hz, 1 H), 7.41 (t, J = 6 Hz, 1 H), 3.31 (m), 1.15 (t, J = 6 Hz, 3 H) ppm. ^{13}C NMR ([D$_4$]MeOH): see the Supporting Information. IR (neat): ṽ = 3297 (N–H str.), 2973 (CH$_3$ str.), 2931 (CH$_2$ str.), 2870 (CH$_3$ str.), 1627 (C=O str.), 1548 (N–H bend.), 1463 (CH$_2$–N str.), 1288 (CH$_3$ str.), 746 (N–C–O str.) cm^{-1}. ESI-HRMS: calcd. 226.111 [M$^+$]; found 226.115.

General Synthesis of Ir^{III} Hemicages: Tripodal ligand (100 mg, 0.14 mmol), IrCl$_3$ (41 mg, 0.14 mmol), and CF$_3$CO$_2$Ag (89 mg, 0.4 mmol) were stirred in ethylene glycol (10 mL) previously purged with nitrogen. After several cycles of argon/vacuum, the resulting mixture was heated to reflux overnight. The reaction mixture was cooled to room temperature, diluted with water, and extracted several times with ethyl acetate. The organic phases were collected, washed with brine, and dried with Na$_2$SO$_4$. The products were then purified by column chromatography (SiO$_2$, CH$_2$Cl$_2$/MeOH, 95:5).

Ir-6 (1): ^{1}H NMR ([D$_2$]CH$_2$Cl$_2$): δ = 7.99 (d, J = 12 Hz, 1 H), 7.96 (d, J = 6 Hz, 1 H), 7.76 (s, 1 H), 7.71 (m, 1 H), 7.02 (d, J = 6 Hz, 1 H), 6.95–6.96 (m, 2 H), 6.34 (t, J = 6 Hz, 1 H), 3.62 (d, J = 18 Hz, 1 H), 3.41 (t, J = 12 Hz, 1 H), 2.91 (t, J = 6 Hz, 1 H), 2.30 (d, J = 12 Hz, 1 H) ppm. ^{13}C NMR ([D$_2$]CH$_2$Cl$_2$): see the Supporting Information. ṽ = IR (neat): 3274 (br., NH str.), 3041 (CH$_2$ str.), 2925 (CH$_2$ str.), 2815 (N–CH$_2$/CH$_2$ str.), 1633 (C=O str.), 1539 (NH bend.), 1471 (CH$_2$–N str.), 748 (N–C–O str.) cm^{-1}. ESI-HRMS: calcd. 880.259 [M + H$^+$]; found 880.260.

Ir-9 (3): ^{1}H NMR ([D$_2$]CH$_2$Cl$_2$): δ = 7.98 (d, J = 6 Hz, 1 H), 7.75 (d, J = 12 Hz, 1 H), 7.72 (d, J = 12 Hz, 1 H), 7.59 (d, J = 6 Hz, 1 H), 7.40 (d, J = 6 Hz, 1 H), 7.33 (s, 1 H), 7.09 (t, J = 6 Hz, 1 H), 6.25 (d, J = 6 Hz, 1 H), 3.90 (t, J = 6 Hz, 1 H), 3.05 (t, J = 12 Hz, 1 H), 2.79 (t, J = 12 Hz, 1 H), 2.37 (d, J = 12 Hz, 1 H) ppm. ^{13}C NMR ([D$_2$]CH$_2$Cl$_2$): see the Supporting Information. IR (neat): ṽ = 3290 (br., NH str.), 3066 (CH$_2$ str.), 2921 (CH$_2$ str.), 2850 (N–CH$_2$/CH$_2$ str.), 1643 (C=O str.), 1540 (NH bend.), 1470 (CH$_2$–N str.), 756 (N–C–O str.) cm^{-1}. ESI-HRMS: calcd. 880.259 [M + H$^+$]; found 880.262.

General Synthesis of Open Ir^{III} Complexes: Ligand (100 mg, 0.42 mmol) and IrCl$_3$ (66 mg, 0.22 mmol) were dissolved in a mixture of 2-ethoxyethanol and water (3:1). After several cycles of argon/vacuum, the mixture was heated to reflux overnight. The reaction mixture was cooled to room temperature, half of the solvent was evaporated, and the resulting solution was poured on ice. The resulting precipitate was filtered, washed with water and diethyl ether, and dried under vacuum. The solid (≈70 mg) was then suspended in toluene, ligand (36 mg, 0.15 mmol) and CF$_3$SO$_3$Ag (80 mg, 0.30 mmol) were added, several cycles argon/vacuum were performed to remove oxygen, and the mixture was heated to reflux overnight under inert atmosphere. The crude was then washed with methanol and then dissolved in CH$_2$Cl$_2$ (10% MeOH), filtered through Celite, and eventually purified by preparative TLC (CH$_2$Cl$_2$/MeOH, 95:5).

Ir-7$_3$ (2): ^{1}H NMR ([D$_7$]DMF): δ = 8.60 (t, J = 6 Hz, 1 H), 8.35 (d, J = 6 Hz, 1 H), 8.31–8.28 (m, 2 H), 7.90 (d, J = 12 Hz, 1 H), 6.87 (t, J = 6 Hz, 1 H), 6.79–6.74 (m, 2 H), 3.27 (quint., J = 6 Hz, 2 H), 1.08 (t, J = 6 Hz, 3 H) ppm. ^{13}C NMR ([D$_7$]DMF): see the Supporting Information. IR (neat): ṽ = 3290 (N–H str.), 3035 (CH$_2$ str.), 2970 (CH$_3$ str.), 2930 (CH$_2$ str.), 2873 (CH$_3$ str.), 1635 (C=O str.), 1540 (N–H bend.), 1473 (CH$_2$–N str.), 1257 (CH$_3$ str.), 748 (N–C–O str.) cm^{-1}. ESI-HRMS: calcd. 891.261 [M + Na$^+$]; found 891.262.

Ir-10$_3$ (4): ^{1}H NMR ([D$_7$]DMF): δ = 8.26 (d, J = 12 Hz, 1 H), 7.92 (t, J = 6 Hz, 1 H), 7.86–7.88 (m, 2 H), 7.63 (d, J = 6 Hz, 1 H), 7.37 (s, 1 H), 7.31 (d, J = 12 Hz, 1 H), 7.20 (t, J = 6 Hz, 1 H), 3.22 (quint., J = 6 Hz, 2 H), 1.05 (t, J = 6 Hz, 3 H) ppm. ^{13}C NMR ([D$_7$]DMF): see the Supporting Information. IR (neat): ṽ = 3297 (N–H str.), 3060 (CH$_2$ str.), 2966 (CH$_3$ str.), 2927 (CH$_2$ str.), 2852 (CH$_3$ str.), 1633 (C=O str.), 1540 (N–H bend.), 1467 (CH$_2$–N str.), 1257 (CH$_3$ str.), 754 (N–C–O str.) cm^{-1}. ESI-HRMS: calcd. 869.279 [M + H$^+$]; found 869.278.

Supporting Information (see footnote on the first page of this article): HH-COSY, HH-ROESY and ^{13}C NMR data, isodensity plots and energies of selected molecular orbitals, excitation energies and oscillator strength of the lowest transitions.

Acknowledgments

M. M. thanks the Alexander Humboldt Fundation for financial support.

---

[1] L. Flamigni, A. Barbieri, C. Sabatini, B. Ventura, F. Barigelletti, *Photochemistry and Photophysics of Coordination Compounds II*, vol. 281, **2007**, pp. 143–203.

[2] A. Tsuboyama, H. Iwawaki, M. Furugori, T. Mukaide, J. Kamatani, S. Igawa, T. Moriyama, S. Miura, T. Takiguchi, S. Okada, M. Hoshino, K. Ueno, *J. Am. Chem. Soc.* **2003**, *125*, 12971–12979.

[3] J. I. Kim, I. S. Shin, H. Kim, J. K. Lee, *J. Am. Chem. Soc.* **2005**, *127*, 1614–1615.

[4] M. A. Baldo, D. F. O'Brien, Y. You, A. Shoustikov, S. Sibley, M. E. Thompson, S. R. Forrest, *Nature* **1998**, *395*, 151–154.

[5] V. Fernandez-Moreira, F. L. Thorp-Greenwood, M. P. Coogan, *Chem. Commun.* **2010**, *46*, 186–202.

[6] A. Ruggi, D. N. Reinhoudt, A. H. Velders, in: *Bioinorganic Medicinal Chemistry* (Ed.: E. Alessio), Wiley-VCH, Weinheim, Germany, **2011**.

[7] D. Crespy, K. Landfester, U. S. Schubert, A. Schiller, *Chem. Commun.* **2010**, *46*, 6651–6662.

[8] J. Kuil, P. Steunenberg, P. T. K. Chin, J. Oldenburg, K. Jalink, A. H. Velders, F. W. B. van Leeuwen, *ChemBioChem* **2011**, *12*, 1897–1903.

[9] J. N. Demas, E. W. Harris, R. P. McBride, *J. Am. Chem. Soc.* **1977**, *99*, 3547–3551.

[10] M. P. Coogan, J. B. Court, V. L. Gray, A. J. Hayes, S. H. Lloyd, C. O. Millet, S. J. A. Pope, D. Lloyd, *Photochem. Photobiol. Sci.* **2010**, *9*, 103–109.

[11] J. N. Demas, D. Diemente, E. W. Harris, *J. Am. Chem. Soc.* **1973**, *95*, 6864–6865.

[12] S. J. Zhang, M. Hosaka, T. Yoshihara, K. Negishi, Y. Iida, S. Tobita, T. Takeuchi, *Cancer Res.* **2010**, *70*, 4490–4498.

[13] A. Ruggi, F. W. B. van Leeuwen, A. H. Velders, *Coord. Chem. Rev.* **2011**, *255*, 2542–2554.

[14] C. Li, M. Yu, Y. Sun, Y. Wu, C. Huang, F. Li, *J. Am. Chem. Soc.* **2011**, *133*, 11231–11239.

[15] P. J. Hay, *J. Phys. Chem. A* **2002**, *106*, 1634–1641.

[16] M. S. Lowry, S. Bernhard, *Chem. Eur. J.* **2006**, *12*, 7970–7977.

[17] F. Barigelletti, L. De Cola, V. Balzani, P. Belser, A. Von Zelewsky, F. Voegtle, F. Ebmeyer, S. Grammenudi, *J. Am. Chem. Soc.* **1989**, *111*, 4662–4668.

[18] A. Ruggi, M. B. Alonso, D. N. Reinhoudt, A. H. Velders, *Chem. Commun.* **2010**, *46*, 6726–6728.

[19] R. F. Beeston, S. L. Larson, M. C. Fitzgerald, *Inorg. Chem.* **1989**, *28*, 4187–4189.

[20] N. Miyaura, A. Suzuki, *Chem. Rev.* **2002**, *95*, 2457–2483.

[21] A. B. Tamayo, B. D. Alleyne, P. I. Djurovich, S. Lamansky, I. Tsyba, N. N. Ho, R. Bau, M. E. Thompson, *J. Am. Chem. Soc.* **2003**, *125*, 7377–7387.

[22] J. Breu, P. Stossel, S. Schrader, A. Starukhin, W. J. Finkenzeller, H. Yersin, *Chem. Mater.* **2005**, *17*, 1745–1752.

[23] K. Nozaki, K. Takamori, Y. Nakatsugawa, T. Ohno, *Inorg. Chem.* **2006**, *45*, 6161–6178.

[24] Experimental values are referred to *fac*-[Ir(ppy)$_3$], see: J. Breu, P. Stossel, S. Schrader, A. Starukhin, W. J. Finkenzeller, H. Yersin, *Chem. Mater.* **2005**, *17*, 1745–1752.

[25] S. Fantacci, F. De Angelis, *Coord. Chem. Rev.*, DOI: 10.1016/j.ccr.2011.1003.1008.

[26] A. Vlcek, S. Zalis, *Coord. Chem. Rev.* **2007**, *251*, 258–287.

[27] S. Lamansky, P. Djurovich, D. Murphy, F. Abdel-Razzaq, H. E. Lee, C. Adachi, P. E. Burrows, S. R. Forrest, M. E. Thompson, *J. Am. Chem. Soc.* **2001**, *123*, 4304–4312.

[28] W. Holzer, A. Penzkofer, T. Tsuboi, *Chem. Phys.* **2005**, *308*, 93–102.

[29] I. Avilov, P. Minoofar, J. Cornil, L. De Cola, *J. Am. Chem. Soc.* **2007**, *129*, 8247–8258.

[30] K. D. Oyler, F. J. Coughlin, S. Bernhard, *J. Am. Chem. Soc.* **2007**, *129*, 210–217.

[31] A. Juris, V. Balzani, F. Barigelletti, S. Campagna, P. Belser, A. Vonzelewsky, *Coord. Chem. Rev.* **1988**, *84*, 85–277.

[32] J. R. Lakowicz, *Principles of Fluorescence Spectroscopy*, Springer, Singapore, **2006**.

[33] Q. G. Mulazzani, H. Sun, M. Z. Hoffman, W. E. Ford, M. A. J. Rodgers, *J. Phys. Chem.* **1994**, *98*, 1145–1150.

[34] A. A. Abdel-Shafi, P. D. Beer, R. J. Mortimer, F. Wilkinson, *Helv. Chim. Acta* **2001**, *84*, 2784–2795.

[35] M. Bodesheim, M. Schutz, R. Schmidt, *Chem. Phys. Lett.* **1994**, *221*, 7–14.

[36] M. Montalti, A. Credi, L. Prodi, M. T. Gandolfi, *Handbook of Photochemistry*, CRC press, Boca Raton, **2006**.

[37] C. T. Lee, W. T. Yang, R. G. Parr, *Phys. Rev. B* **1988**, *37*, 785–789.

[38] A. D. Becke, *J. Chem. Phys.* **1993**, *98*, 5648–5652.

[39] M. M. Francl, W. J. Pietro, W. J. Hehre, J. S. Binkley, M. S. Gordon, D. J. Defrees, J. A. Pople, *J. Chem. Phys.* **1982**, *77*, 3654–3665.

[40] M. Cossi, N. Rega, G. Scalmani, V. Barone, *J. Comput. Chem.* **2003**, *24*, 669–681.

[41] M. Cossi, V. Barone, *J. Chem. Phys.* **2001**, *115*, 4708–4717.

[42] V. Barone, M. Cossi, *J. Phys. Chem. A* **1998**, *102*, 1995–2001.

[43] R. E. Stratmann, G. E. Scuseria, M. J. Frisch, *J. Chem. Phys.* **1998**, *109*, 8218–8224.

[44] M. E. Casida, C. Jamorski, K. C. Casida, D. R. Salahub, *J. Chem. Phys.* **1998**, *108*, 4439–4449.

[45] M. J. Frisch, G. W. Trucks, H. B. Schlegel, G. E. Scuseria, M. A. Robb, J. R. Cheeseman, G. Scalmani, V. Barone, B. Mennucci, G. A. Petersson, H. Nakatsuji, M. Caricato, X. Li, H. P. Hratchian, A. F. Izmaylov, J. Bloino, G. Zheng, J. L. Sonnenberg, M. Hada, M. Ehara, K. Toyota, R. Fukuda, J. Hasegawa, M. Ishida, T. Nakajima, Y. Honda, O. Kitao, H. Nakai, T. Vreven, J. A. Montgomery Jr, J. E. Peralta, F. Ogliaro, M. Bearpark, J. J. Heyd, E. Brothers, K. N. Kudin, V. N. Staroverov, R. Kobayashi, J. Normand, K. Raghavachari, A. Rendell, J. C. Burant, S. S. Iyengar, J. Tomasi, M. Cossi, N. Rega, J. M. Millam, M. Klene, J. E. Knox, J. B. Cross, V. Bakken, C. Adamo, J. Jaramillo, R. Gomperts, R. E. Stratmann, O. Yazyev, A. J. Austin, R. Cammi, C. Pomelli, J. W. Ochterski, R. L. Martin, K. Morokuma, V. G. Zakrzewski, G. A. Voth, P. Salvador, J. J. Dannenberg, S. Dapprich, A. D. Daniels, Ö. Farkas, J. B. Foresman, J. V. Ortiz, J. Cioslowski, D. J. Fox, *Gaussian 09*, revision B.1, Gaussian, Inc., Wallingford CT, **2009**.

[46] Y. Gong, H. W. Pauls, *Synlett* **2000**, 829–831.

[47] A. J. Bard, L. R. Faulkner, *Electrochemical Methods, Fundamentals and Applications*, Wiley, New York, **2001**.

Received: November 24, 2011